Nonlinear Beamforming Based on Group Sparsity for Phased Array Weather Radar

Daichi KITAHARA† Akira HIRABAYASHI† Eiichi YOSHIKAWA‡
Hiroshi KIKUCHI* Tomoo USHIO*

† College of Information Science and Engineering, Ritsumeikan University
‡ Aeronautical Technology Directorate, Japan Aerospace Exploration Agency
∗ Department of Aerospace Engineering, Tokyo Metropolitan University

Abstract Recently, we proposed a *nonlinear* beamforming method for a phased array weather radar (PAWR). In this method, by evaluating two properties of signals from distributed targets with group ℓ_1-norms, beamforming performance can be greatly improved compared to *linear* methods. However, the reconstructed power spectral density still has several peaks although the true density has only one peak. In this paper, as a continuation of our nonlinear beamforming, we propose to modify the cost function used in the previous method. Specifically, we roughly estimate the support of the power spectral density and use a novel group ℓ_1-norm having a large weight for the nonsupport region. Simulations using real PAWR data show that the proposed method accurately reconstructs the power spectral density.

1 Introduction

Phased array weather radar (PAWR) [1], [2] has been developed for fast detection of hazardous weather phenomena such as a thunderstorm with heavy rain. A classical parabolic radar transmits a pencil beam and receives the backscattered signals within a *narrow* range of elevation angles. On the other hand, a PAWR transmits a fan beam and receives the backscattered signals within a *wide* range of elevation angles simultaneously by an antenna array. Then, the backscattered signals within the *narrow* ranges are reconstructed from the received signals of the antenna array by digital *beamforming* [3]–[6]. This is the key technology in the PAWR because it gets rid of the mechanical vertical scan and hence the temporal resolution was drastically improved in weather observation. Indeed, the PAWR developed at Osaka University [2] can observe the weather in a hemisphere of a radius 60 kilometers in 30 seconds, while the classical parabolic radar requires 5 to 10 minutes for a similar observation [7].

Major beamforming methods [3]–[5] reconstruct the signal arriving from each elevation as a complex weighted sum of the received signals. In particular, Capon beamforming [4] is a famous method that can adaptively reduce the influence of sidelobes if a sufficient number of pulses are transmitted. For fast weather observation, however, the number of pulses should be as small as possible. To deal with such a situation, the minimum mean square error (MMSE) beamforming [5] was proposed. In this method, differently from Capon's method, the sample covariance matrix of the received signals is not computed, and hence the signal arriving from each elevation can be robustly reconstructed even if the number of pulses is small. Such beamforming methods were developed originally for observation of *point targets*, but targets of the PAWR are *distributed targets* such as raindrops. In this case, the number of the backscattered signals is often very large, and the spatial resolution of the above *linear* methods [3]–[5] is limited, i.e., fine variation of the reflection intensity corresponding to precipitation profile cannot be captured.

To overcome the limitation of the *linear* methodology, we recently proposed a *nonlinear* beamforming method [6]. In this method, we considered the beamforming as an inverse problem and solved it by utilizing two properties of signals from distributed targets. One is the continuity of the reflection intensity in the temporal and spatial domains. The other is the narrow bandwidth in the frequency domain. We expressed these properties as group-sparsity of certain matrices and reconstructed the signals by minimizing a convex cost function that consists of the data-fidelity term and two group ℓ_1-norms. This nonlinear method greatly improves the estimation accuracy compared to the linear methods. However, the reconstructed power spectral densities often have several peaks although the true densities have only one peak.

As a continuation of the nonlinear beamforming in [6], in this paper, we propose to minimize a modified convex cost function. First, in the frequency domain, we roughly estimate the support of each signal by using the estimation results of [6]. Second, we replace the group ℓ_1-norm based on the continuity of the reflection intensity with a weighted group ℓ_1-norm. One group having a small weight corresponds to the estimated support area. The other having a large weight corresponds to the nonsupport area. The modified cost function can be effectively minimized with the alternating direction method of multipliers (ADMM) [8]. Numerical experiments show the effectiveness of the proposed method in comparison with the linear and the previous nonlinear methods.

2 Preliminaries

Let $\mathbb{R}$ and $\mathbb{C}$ be the sets of all real numbers and complex numbers, respectively. We use $j \in \mathbb{C}$ to denote the imaginary unit, i.e., $j = \sqrt{-1}$. For any $x \in \mathbb{C}$, $\bar{x}$ denotes its complex conjugate, and $|x| := \sqrt{x\bar{x}}$ denotes its absolute value. We write vectors with lowercase boldface letters and matrices with capital letters. We use $I_n \in \mathbb{R}^{n\times n}$ to denote the identity matrix of order n. The transpose and the Hermitian transpose of vectors or matrices are respectively expressed as $(\cdot)^{\mathrm{T}}$ and $(\cdot)^{\mathrm{H}}$. For any $\boldsymbol{x} := (x_1, x_2, \ldots, x_n)^{\mathrm{T}} \in \mathbb{C}^n$, the ℓ_2-norm (or

the Euclidean norm) is defined by $\|\boldsymbol{x}\|_2 := \sqrt{\sum_{i=1}^{n} |x_i|^2}$, and a group ℓ_1-norm with non-overlapping groups is defined by $\|\boldsymbol{x}\|_1^G := \sum_{i=1}^{n_G} \|\boldsymbol{x}_{\mathcal{G}_i}\|_2$, where $\boldsymbol{x}_{\mathcal{G}_i}$ $(i = 1, 2, \ldots, n_G)$ are sub-vectors of $\boldsymbol{x}$ divided by index sets $\mathcal{G}_i$ $(i = 1, 2, \ldots, n_G)$ s.t. $\bigcup_{i=1}^{n_G} \mathcal{G}_i = \{1, 2, \ldots, n\}$ and $\mathcal{G}_i \cap \mathcal{G}_{i'} = \varnothing$ $(i \neq i')$. We use $E[\cdot]$ to denote the expected values of random variables.

2.1 Signal Model

First of all, we give a signal model for the observation of K *point targets*. Let a PAWR have an N-element uniform linear array with the inter-element spacing $d\,[\mathrm{m}]$. A plane wave signal scattered from the kth point target impinges on the antenna array at an angle $\theta_k^\star \in [\theta_{\min}, \theta_{\max}]$ $(\theta_1^\star < \theta_2^\star < \cdots < \theta_K^\star\,[\mathrm{rad}])$. Then, the lth time sample of the received signal $\boldsymbol{y}_l \in \mathbb{C}^N$ is given by

$$\boldsymbol{y}_l = \sum_{k=1}^{K} x_{k,l}^\star \boldsymbol{a}(\theta_k^\star) + \boldsymbol{v}_l \qquad (l = 1, 2, \ldots, L), \tag{1}$$

where $x_{k,l}^\star \in \mathbb{C}$ is the lth sample of the kth plane wave signal s.t. $E[x_{k,l}^\star] = 0$, $\boldsymbol{a}(\theta_k^\star) \in \mathbb{C}^N$ is the steering vector defined as

$$\boldsymbol{a}(\theta) := \big(1, e^{-j\frac{2\pi d \sin\theta}{\lambda}}, e^{-j\frac{4\pi d \sin\theta}{\lambda}}, \ldots, e^{-j\frac{2(N-1)\pi d \sin\theta}{\lambda}}\big)^{\mathrm{T}}$$

with the carrier wavelength $\lambda\,[\mathrm{m}]$, and $\boldsymbol{v}_l \in \mathbb{C}^N$ is the white Gaussian noise of covariance matrix $R_v := E[\boldsymbol{v}_l \boldsymbol{v}_l^{\mathrm{H}}] = \sigma_v^2 I_N$.

On the other hand, our targets such as raindrops are called *distributed targets*, which are supposed to exist continuously (strictly speaking, there are a number of raindrops within the antenna beamwidth). Let us observe the distributed targets while dividing the whole angular interval $[\theta_{\min}, \theta_{\max}]$ into M sub-intervals $[\theta_m - \frac{\Delta\theta}{2}, \theta_m + \frac{\Delta\theta}{2}]$, where $\Delta\theta := \frac{\theta_{\max} - \theta_{\min}}{M}$ and $\theta_m := \theta_{\min} + (m - \frac{1}{2})\Delta\theta$ $(m = 1, 2, \ldots, M)$. Therefore, instead of (1), we use the following signal model

$$\boldsymbol{y}_l = \sum_{m=1}^{M} x_{m,l} \boldsymbol{s}_m + \boldsymbol{v}_l = S\boldsymbol{x}_l + \boldsymbol{v}_l, \tag{2}$$

where $x_{m,l} \in \mathbb{C}$ s.t. $E[x_{m,l}] = 0$ is the lth sample of the sum of plane wave signals in the sub-interval $[\theta_m - \frac{\Delta\theta}{2}, \theta_m + \frac{\Delta\theta}{2}]$, $\boldsymbol{x}_l := (x_{1,l}, x_{2,l}, \ldots, x_{M,l})^{\mathrm{T}} \in \mathbb{C}^M$, $\boldsymbol{s}_m := \boldsymbol{a}(\theta_m) \in \mathbb{C}^N$, and $S := (\boldsymbol{s}_1, \boldsymbol{s}_2, \ldots, \boldsymbol{s}_M) \in \mathbb{C}^{N \times M}$. We can derive (1) from (2) by redefining $K\,(\leq M)$ as the number of the sub-intervals $[\theta_m - \frac{\Delta\theta}{2}, \theta_m + \frac{\Delta\theta}{2}]$ where plane wave signals exist, and $\theta_k^\star$ as the centers of such sub-intervals. In the PAWR system, θ_m means the mth elevation angle, and the reflection intensity

$$\boldsymbol{p} := \big(E\big[|x_{1,l}|^2\big], E\big[|x_{2,l}|^2\big], \ldots, E\big[|x_{M,l}|^2\big]\big)^{\mathrm{T}} \in \mathbb{R}^M$$

corresponds to precipitation profile in the elevation angles.

2.2 Linear Beamforming

Beamforming is an estimation problem of $\boldsymbol{x}_l$ from $\boldsymbol{y}_l$ in (2). Major beamforming methods estimate $\boldsymbol{x}_l$ by multiplying complex weights $\boldsymbol{w}_m \in \mathbb{C}^N$ $(m = 1, 2, \ldots, M)$ and $\boldsymbol{y}_l$ as

$$\begin{aligned}\widehat{\boldsymbol{x}}_l &:= (\widehat{x}_{1,l}, \widehat{x}_{2,l}, \ldots, \widehat{x}_{M,l})^{\mathrm{T}} \\ &:= (\boldsymbol{w}_1^{\mathrm{H}} \boldsymbol{y}_l, \boldsymbol{w}_2^{\mathrm{H}} \boldsymbol{y}_l, \ldots, \boldsymbol{w}_M^{\mathrm{H}} \boldsymbol{y}_l)^{\mathrm{T}} = W \boldsymbol{y}_l.\end{aligned} \tag{3}$$

In this paper, the methods based on (3) are called the *linear beamforming*. Note that the least squares (LS) method

$$\widehat{\boldsymbol{x}}_{\mathrm{LS},l} := W_{\mathrm{LS}}\, \boldsymbol{y}_l := S^\dagger \boldsymbol{y}_l \tag{4}$$

does not necessarily work well, even if $N \geq M$, because S is ill-conditioned when $\Delta\theta$ is smaller than the antenna beamwidth which is determined by the antenna size, where $S^\dagger \in \mathbb{C}^{M \times N}$ is the Moore-Penrose pseudoinverse of S. In the following, we introduce three major linear methods, *Fourier (FR) beamforming* [3], *Capon (CP) beamforming* [4], and *MMSE beamforming* [5].

2.2.1 FR Beamforming

FR beamforming [3] is the most basic method. Its complex weight vector is defined by

$$\boldsymbol{w}_{\mathrm{FR},m} := \frac{\boldsymbol{s}_m}{N} \tag{5}$$

independently of $\boldsymbol{y}_l$. The weight vector $\boldsymbol{w}_{\mathrm{FR},m}$ is a matched filter maximizing the signal-to-noise ratio $\frac{E[|x_{m,l}\boldsymbol{w}_m^{\mathrm{H}}\boldsymbol{s}_m|^2]}{E[|\boldsymbol{w}_m^{\mathrm{H}}\boldsymbol{v}_l|^2]}$. However, from

$$\widehat{x}_{\mathrm{FR},m,l} := \frac{\boldsymbol{s}_m^{\mathrm{H}}}{N}\boldsymbol{y}_l = x_{m,l} + \frac{1}{N}\sum_{\theta_k^\star \neq \theta_m} x_{k,l}^\star \boldsymbol{s}_m^{\mathrm{H}} \boldsymbol{a}(\theta_k^\star) + \frac{1}{N}\boldsymbol{s}_m^{\mathrm{H}}\boldsymbol{v}_l,$$

the precipitation profile is overestimated for many elevation angles θ_m since

$$\widehat{p}_{\mathrm{FR},m} := \frac{1}{L}\sum_{l=1}^{L} |\widehat{x}_{\mathrm{FR},m,l}|^2 \gg E\big[|x_{m,l}|^2\big] + \frac{\sigma_v^2}{N}$$

often holds for m satisfying $\exists \theta_k^\star \neq \theta_m$ $|\boldsymbol{s}_m^{\mathrm{H}} \boldsymbol{a}(\theta_k^\star)| \not\approx 0$.

2.2.2 CP Beamforming

CP beamforming [4] is a data-dependent method which minimizes $\frac{1}{L}\sum_{l=1}^{L} |\widehat{x}_{m,l}|^2 = \boldsymbol{w}_m^{\mathrm{H}} \widehat{R}_y \boldsymbol{w}_m$ under the condition $\boldsymbol{w}_m^{\mathrm{H}} \boldsymbol{s}_m = 1$ to avoid the above overestimation, where $\widehat{R}_y := \frac{1}{L}\sum_{l=1}^{L} \boldsymbol{y}_l \boldsymbol{y}_l^{\mathrm{H}} \in \mathbb{C}^{N \times N}$ is the sample covariance matrix of the zero-mean random variable $\boldsymbol{y}_l$. The weight vector $\boldsymbol{w}_{\mathrm{CP},m}$ is defined as the solution of the optimization problem

$$\underset{\boldsymbol{w}_m}{\text{minimize}}\ \boldsymbol{w}_m^{\mathrm{H}} \widehat{R}_y \boldsymbol{w}_m \qquad \text{subject to } \boldsymbol{w}_m^{\mathrm{H}} \boldsymbol{s}_m = 1$$

by

$$\boldsymbol{w}_{\mathrm{CP},m} := \frac{\widehat{R}_y^{-1}\boldsymbol{s}_m}{\boldsymbol{s}_m^{\mathrm{H}}\widehat{R}_y^{-1}\boldsymbol{s}_m} \tag{6}$$

if $L \geq N$ (strictly speaking, if $\mathrm{rank}(\widehat{R}_y) = N$). Particularly, if $N \geq K + 1$ and L is sufficiently large, then we have

$$\widehat{p}_{\mathrm{CP},m} := \frac{1}{L}\sum_{l=1}^{L} |\widehat{x}_{\mathrm{CR},m,l}|^2 \approx E\big[|x_{m,l}|^2\big] + \sigma_v^2 \|\boldsymbol{w}_{\mathrm{CP},m}\|_2^2$$

for all m since $\forall \theta_k^\star \neq \theta_m$ $|\boldsymbol{w}_{\mathrm{CP},m}^{\mathrm{H}} \boldsymbol{a}(\theta_k^\star)| \approx 0$ holds. However, if L is not large, then the precipitation profile is often underestimated [5], and if $L < N$, $\widehat{R}_y^{-1}$ cannot be computed.

2.2.3 MMSE Beamforming

MMSE beamforming [5] was developed to improve the estimation accuracy in case of small L, including $L < N$. This method approximately solves the optimization problem

$$\underset{\boldsymbol{w}_m}{\text{minimize}}\ E\big[|x_{m,l} - \boldsymbol{w}_m^{\mathrm{H}} \boldsymbol{y}_l|^2\big] \qquad \text{subject to } \boldsymbol{w}_m^{\mathrm{H}} \boldsymbol{s}_m = 1.$$

Assuming $E[x_{m,l}\bar{x}_{m',l}] = E[x_{m,l}]E[\bar{x}_{m',l}] = 0$ if $m \neq m'$, the exact solution of the above optimization problem is

$$\boldsymbol{w}_{\mathrm{MMSE},m} := \frac{R_y^{-1}\boldsymbol{s}_m}{\boldsymbol{s}_m^{\mathrm{H}} R_y^{-1}\boldsymbol{s}_m}, \tag{7}$$

where $R_y := E[\boldsymbol{y}_l \boldsymbol{y}_l^{\mathrm{H}}]$ is the covariance matrix of $\boldsymbol{y}_l$. By using the covariance matrix $R_x := E[\boldsymbol{x}_l \boldsymbol{x}_l^{\mathrm{H}}]$ of $\boldsymbol{x}_l$, R_y is expressed as $R_y = SR_xS^{\mathrm{H}} + \sigma_v^2 I_N$. Moreover, $R_x = \mathrm{diag}(\boldsymbol{p})$ can be approximated by $\widehat{R}_x \odot I_M := (\frac{1}{L}\sum_{l=1}^{L} \boldsymbol{x}_l \boldsymbol{x}_l^{\mathrm{H}}) \odot I_M$, where $\odot$ denotes the Hadamard product. As a result, the weight vector $\boldsymbol{w}_{\mathrm{MMSE},m}$ in (7) is approximated, from the initial estimate $\widehat{\boldsymbol{x}}_{\mathrm{MMSE},l}^{(0)} = \widehat{\boldsymbol{x}}_{\mathrm{FR},l} = S^{\mathrm{H}}\boldsymbol{y}_l/N$, by computing

$$\begin{aligned}
R_x^{(i)} &= \left(\frac{1}{L}\sum_{l=1}^{L} \widehat{\boldsymbol{x}}_{\mathrm{MMSE},l}^{(i)} \widehat{\boldsymbol{x}}_{\mathrm{MMSE},l}^{(i)\mathrm{H}}\right) \odot I_M \\
R_y^{(i)} &= SR_x^{(i)}S^{\mathrm{H}} + \sigma_v^2 I_N \\
\boldsymbol{w}_{\mathrm{MMSE},m}^{(i+1)} &= \frac{R_y^{(i)-1}\boldsymbol{s}_m}{\boldsymbol{s}_m^{\mathrm{H}} R_y^{(i)-1}\boldsymbol{s}_m} \qquad (m = 1, 2, \ldots, M) \\
\widehat{\boldsymbol{x}}_{\mathrm{MMSE},l}^{(i+1)} &= W_{\mathrm{MMSE}}^{(i+1)}\boldsymbol{y}_l \qquad (l = 1, 2, \ldots, L)
\end{aligned} \tag{8}$$

for $i \geq 0$ until $\delta^{(i+1)} = \frac{1}{M}\sum_{m=1}^{M} \frac{\sum_{l=1}^{L} |\widehat{x}_{\mathrm{MMSE},m,l}^{(i+1)} - \widehat{x}_{\mathrm{MMSE},m,l}^{(i)}|^2}{\sum_{l=1}^{L} |\widehat{x}_{\mathrm{MMSE},m,l}^{(i)}|^2}$ becomes sufficiently small. In this method, even for small L, R_y can be stably estimated. However, if K is close to N or larger than N, then the estimation accuracy degrades, i.e., fine variation of the precipitation profile cannot be captured.

3 Nonlinear Beamforming via Convex Optimization Based on Group-Sparsity

In this section, at first, we introduce our previous *nonlinear beamforming* method in [6]. Then, we propose its improved version by modifying the convex cost function with the use of the estimation results of [6].

3.1 Nonlinear Beamforming in [6]

First, we gather $\boldsymbol{x}_l$ and $\boldsymbol{y}_l$ into $X := (\boldsymbol{x}_1, \boldsymbol{x}_2, \ldots, \boldsymbol{x}_L) = (\widetilde{\boldsymbol{x}}_1, \widetilde{\boldsymbol{x}}_2, \ldots, \widetilde{\boldsymbol{x}}_M)^{\mathrm{T}} \in \mathbb{C}^{M\times L}$ and $Y := (\boldsymbol{y}_1, \boldsymbol{y}_2, \ldots, \boldsymbol{y}_L) \in \mathbb{C}^{N\times L}$, where $\widetilde{\boldsymbol{x}}_m := (x_{m,1}, x_{m,2}, \ldots, x_{m,L})^{\mathrm{T}} \in \mathbb{C}^L$. Then the beamforming is translated into an estimation problem of X from Y, and the data fidelity in (2) can be evaluated by the Frobenius norm as

$$\|Y - SX\|_{\mathrm{F}}^2 := \sum_{l=1}^{L} \|\boldsymbol{y}_l - S\boldsymbol{x}_l\|_2^2. \tag{9}$$

In [6], we expressed two characteristics on the signal $\widetilde{\boldsymbol{x}}_m$ as group-sparsity of certain two matrices, and solved a convex optimization problem based on (9) and the double group-sparsity. In the following, we summarize the characteristics on $\widetilde{\boldsymbol{x}}_m$ and the convex cost function used in [6].

3.1.1 Continuity of the Precipitation Profile

Many PAWR systems employ contiguous pair sampling [9]. In such systems, the pulse repetition time (PRT) is designed by $T_{\mathrm{PRT}} := \frac{2r_{\max}}{c}\,[\mathrm{s}]$, where $r_{\max}\,[\mathrm{m}]$ is the maximum range to be observed and $c\,[\mathrm{m/s}]$ is the speed of light. For example, the PAWR system developed at Osaka University can observe the weather in a hemisphere of a radius 60 kilometers [2] and hence the PRT is $T_{\mathrm{PRT}} \approx 0.0004\,[\mathrm{s}]$. If L is not large, the total observation time $LT_{\mathrm{PRT}}\,[\mathrm{s}]$ is sufficiently short to consider $\theta_k^\star$ to be constant for the time index $l = 1, 2, \ldots, L$. Therefore, $\widetilde{\boldsymbol{x}}_m$ becomes a dense vector if $\theta_m = \theta_k^\star$ for some k, and $\widetilde{\boldsymbol{x}}_m = \boldsymbol{0}$ otherwise. Furthermore, from the continuity of the precipitation profile, if $\widetilde{\boldsymbol{x}}_m = \boldsymbol{0}$, it is highly possible that $\widetilde{\boldsymbol{x}}_{m-1}$ and $\widetilde{\boldsymbol{x}}_{m+1}$ are also $\boldsymbol{0}$. This property can be expressed as group-sparsity of the matrix X and evaluated by a group ℓ_1-norm

$$\|X\|_1^{G_1} := \sum_{i=1}^{M/q} \left\|(\widetilde{\boldsymbol{x}}_{(i-1)q+1}^{\mathrm{T}}, \widetilde{\boldsymbol{x}}_{(i-1)q+2}^{\mathrm{T}}, \ldots, \widetilde{\boldsymbol{x}}_{iq}^{\mathrm{T}})^{\mathrm{T}}\right\|_2 \tag{10}$$

with the use of a factor $q \geq 1$ of M.

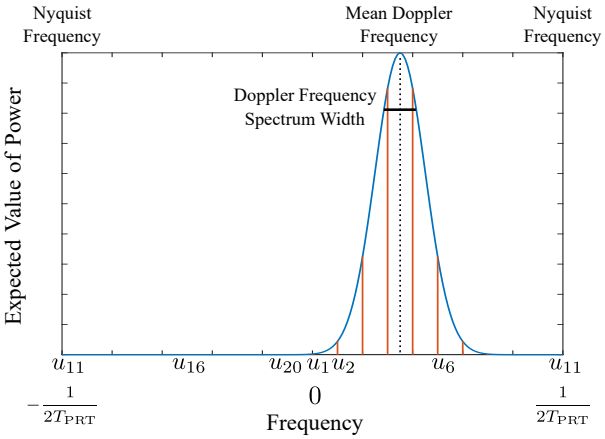

Figure 1: Power spectral density function of the backscattered signals from distributed targets. Blue line depicts the power spectral density function. Red lines depicts $E[|u_{m,l}|^2]$ $(l = 1, 2, \ldots, L := 20)$. In the above graph, the index m is omitted for simplicity.

3.1.2 Narrow Bandwidth of the Backscatterd Signals

The power spectral density of the backscattered signals from the distributed targets, such as raindrops, fog droplets and cloud droplets, can be modeled by a Gaussian function according to the central limit theorem [10], [11]. The first raw moment of the normalized power spectral density, i.e., the center of the above Gaussian function, is called the *mean Doppler frequency* (or the *mean Doppler shift*). The square root of the second central moment, i.e., the standard division of the Gaussian function, is called the *Doppler frequency spectrum width* (see Fig. 1).

Define the normalized discrete Fourier transform matrix by $F := \frac{1}{\sqrt{L}}(\boldsymbol{f}_0, \boldsymbol{f}_1, \ldots, \boldsymbol{f}_{L-1}) \in \mathbb{C}^{L\times L}$, where

$$\boldsymbol{f}_i := \left(1, e^{-j\frac{2\pi i}{L}}, e^{-j\frac{4\pi i}{L}}, \ldots, e^{-j\frac{2(L-1)\pi i}{L}}\right)^{\mathrm{T}} \in \mathbb{C}^L.$$

Then the vector $\boldsymbol{u}_m := F\widetilde{\boldsymbol{x}}_m = (u_{m,1}, u_{m,2}, \ldots, u_{m,L})^{\mathrm{T}} \in \mathbb{C}^L$ is group-sparse. This is because the indices l having large $|u_{m,l}|$ concentrate in the vicinity of the mean Doppler frequency as shown in Fig. 1. However, we cannot specify the center and the width of such a group because the mean Doppler frequency and the spectrum width are different for each elevation angle θ_m. Alternatively, we divide $\boldsymbol{u}_m$ into

L overlapping blocks of size b:

$$\begin{cases} \boldsymbol{b}_{m,1} := (u_{m,1}, u_{m,2}, \dots, u_{m,b})^{\mathrm{T}} \in \mathbb{C}^b \\ \boldsymbol{b}_{m,2} := (u_{m,2}, u_{m,3}, \dots, u_{m,b+1})^{\mathrm{T}} \in \mathbb{C}^b \\ \qquad \vdots \\ \boldsymbol{b}_{m,L-b+1} := (u_{m,L-b+1}, u_{m,L-b+2}, \dots, u_{m,L})^{\mathrm{T}} \in \mathbb{C}^b \\ \boldsymbol{b}_{m,L-b+2} := (u_{m,L-b+2}, \dots, u_{m,L}, u_{m,1})^{\mathrm{T}} \in \mathbb{C}^b \\ \qquad \vdots \\ \boldsymbol{b}_{m,L} := (u_{m,L}, u_{m,1}, \dots, u_{m,b-1})^{\mathrm{T}} \in \mathbb{C}^b \end{cases}$$

under the periodic boundary condition. Therefore, if we define a matrix $B \in \mathbb{R}^{bL \times L}$ satisfying

$$BF\widetilde{\boldsymbol{x}}_m = B\boldsymbol{u}_m = (\boldsymbol{b}_{m,1}^{\mathrm{T}}, \boldsymbol{b}_{m,2}^{\mathrm{T}}, \dots, \boldsymbol{b}_{m,L}^{\mathrm{T}})^{\mathrm{T}} \in \mathbb{C}^{bL},$$

the matrix BFX^{T} becomes group-sparse without overlapping, and this property can be evaluated by a group ℓ_1-norm

$$\|BFX^{\mathrm{T}}\|_1^{G_2} := \sum_{m=1}^{M} \sum_{l=1}^{L} \|\boldsymbol{b}_{m,l}\|_2. \tag{11}$$

In [6], on the basis of (9), (10), and (11), we estimated X from Y by solving a convex optimization problem

$$\underset{X}{\text{minimize}}\ \frac{1}{2}\|Y - SX\|_{\mathrm{F}}^2 + \nu_1 \|X\|_1^{G_1} + \nu_2 \|BFX^{\mathrm{T}}\|_1^{G_2} \tag{12}$$

with the use of ADMM [8] (see Appendix), where $\nu_1 > 0$ and $\nu_2 > 0$. This nonlinear method greatly improved the estimation accuracy compared to the linear methods [3]–[5].

3.2 The Proposed Nonlinear Beamforming

Although the true power spectral densities have only one peak as shown in Fig. 1, the reconstructed densities by the method in [6] often have several peaks (mainly two peaks). Therefore, we propose to modify the cost function in (12) so that the power spectral densities reconstructed from the optimal solution will have only one peak. For this purpose, first we roughly estimate the vicinity of the mean Doppler frequency by using the estimation results of [6] as follows.

1. Obtain the minimizer $\widehat{X}$ of (12) by ADMM.
2. Compute $\widehat{U} := (\widehat{\boldsymbol{u}}_1, \widehat{\boldsymbol{u}}_2, \dots, \widehat{\boldsymbol{u}}_m) = F\widehat{X}^{\mathrm{T}}$.
3. For each $\widehat{\boldsymbol{u}}_m$, replace components, whose absolute values are lower than a certain threshold τ, with 0s.
4. For each replaced $\widehat{\boldsymbol{u}}_m$, detect blocks of any size, whose all components are nonzero, under the periodic boundary condition, and compute the norms of such blocks.
5. Estimate the support of $\boldsymbol{u}_m$ with the use of the block having the largest norm, which is computed in Step 4.

Second, we divide $\boldsymbol{u}_m$ into two groups (i) $\boldsymbol{v}_m$ corresponding the estimated support area and (ii) $\boldsymbol{v}_m^{\mathrm{C}}$ corresponding the nonsupport area (i.e., the complement of the support). To be more specific, $\boldsymbol{v}_m$ and $\boldsymbol{v}_m^{\mathrm{C}}$ are expressed as

$$\begin{cases} \boldsymbol{v}_m = (u_{m,\mathrm{s}}, u_{m,\mathrm{s}+1}, \dots, u_{m,\mathrm{e}})^{\mathrm{T}} \\ \boldsymbol{v}_m^{\mathrm{C}} = (u_{m,1}, u_{m,2}, \dots, u_{m,\mathrm{s}-1}, u_{m,\mathrm{e}+1}, , \dots, u_{m,L})^{\mathrm{T}} \end{cases}$$

or

$$\begin{cases} \boldsymbol{v}_m = (u_{m,1}, u_{m,2}, \dots, u_{m,\mathrm{e}}, u_{m,\mathrm{s}}, u_{m,\mathrm{s}+1}, \dots, u_{m,L})^{\mathrm{T}} \\ \boldsymbol{v}_m^{\mathrm{C}} = (u_{m,\mathrm{e}+1}, u_{m,\mathrm{e}+2}, \dots, u_{m,\mathrm{s}-1})^{\mathrm{T}} \end{cases}$$

with the use of the start index s and the end index e of the estimated support area. Then, this support property can be evaluated by a weighted group ℓ_1-norm

$$\|FX^{\mathrm{T}}\|_{1,\boldsymbol{\kappa}}^{G_3} := \sum_{m=1}^{M} \big(\kappa_{m,1}\|\boldsymbol{v}_m\|_2 + \kappa_{m,2}\|\boldsymbol{v}_m^{\mathrm{C}}\|_2\big), \tag{13}$$

where $\boldsymbol{\kappa} := (\kappa_{1,1}, \kappa_{1,2}, \kappa_{2,1}, \dots, \kappa_{M,2})^{\mathrm{T}} \in \mathbb{R}^{2M}$, $\kappa_{m,1} > 0$ is a small weight and $\kappa_{m,2} > \kappa_{m,1}$ is a large weight.

At this point, if elevation angles θ_m satisfying $\widetilde{\boldsymbol{x}}_m = \boldsymbol{0}$ have been detected by $\boldsymbol{v}_m^{\mathrm{C}} = \boldsymbol{u}_m$, the group ℓ_1-norm in (10) is no longer required. Therefore, on the cost function, we replace (10) with the weighted group ℓ_1-norm in (13), and re-estimate X by solving a convex optimization problem

$$\underset{X}{\text{minimize}}\ \frac{1}{2}\|Y - SX\|_{\mathrm{F}}^2 + \nu\|BFX^{\mathrm{T}}\|_1^{G_2} + \|FX^{\mathrm{T}}\|_{1,\boldsymbol{\kappa}}^{G_3} \tag{14}$$

with the use of ADMM, where $\nu > 0$. The problem in (14) is expressed as an ADMM-form

$$\begin{aligned} &\underset{X \in \mathcal{X}, Z \in \mathcal{Z}}{\text{minimize}}\ \frac{1}{2}\|Y - SX\|_{\mathrm{F}}^2 + \nu\|Z_1\|_1^{G_2} + \|Z_2\|_{1,\boldsymbol{\kappa}}^{G_3} \\ &\text{subject to } Z := \begin{bmatrix} Z_1 \\ Z_2 \end{bmatrix} = \mathcal{L}(X) := \begin{bmatrix} BF \circ \mathcal{T} \\ F \circ \mathcal{T} \end{bmatrix}(X), \end{aligned} \tag{15}$$

where $\mathcal{X} := \mathbb{C}^{M \times L}$, $\mathcal{Z} := \mathbb{C}^{bL \times M} \times \mathbb{C}^{L \times M}$, $\mathcal{T}$ is the transpose operator, $\circ$ denotes the composition of mappings, and convex functions f and g in (21) are respectively defined by $f(X) := \frac{1}{2}\|Y - SX\|_{\mathrm{F}}^2$ and $g(Z) := \nu\|Z_1\|_1^{G_2} + \|Z_2\|_{1,\boldsymbol{\kappa}}^{G_3}$.

On the first line in (22), since X is updated as the solution of a least squares problem, the solution $X^{(i+1)}$ satisfies

$$\left(S^{\mathrm{H}}S + \frac{1}{\gamma}\,\mathcal{L}^* \circ \mathcal{L}\right)(X^{(i+1)}) = S^{\mathrm{H}}Y + \frac{1}{\gamma}\,\mathcal{L}^*(Z^{(i)} - D^{(i)}), \tag{16}$$

where $\mathcal{L}^* : \mathcal{Z} \to \mathcal{X}$ is the adjoint operator of $\mathcal{L}$, defined by $\mathcal{L}^*(Z) := \mathcal{T} \circ F^{\mathrm{H}}B^{\mathrm{T}}(Z_1) + \mathcal{T} \circ F^{\mathrm{H}}(Z_2) = (Z_1^{\mathrm{T}}B + Z_2^{\mathrm{T}})F^{\mathrm{H}}$. Moreover, the composite mapping $\mathcal{L}^* \circ \mathcal{L}$ is expressed as

$$\begin{aligned} \mathcal{L}^* \circ \mathcal{L} &= \begin{bmatrix} \mathcal{T} \circ F^{\mathrm{H}}B^{\mathrm{T}} & \mathcal{T} \circ F^{\mathrm{H}} \end{bmatrix} \begin{bmatrix} BF \circ \mathcal{T} \\ F \circ \mathcal{T} \end{bmatrix} \\ &= \mathcal{T} \circ F^{\mathrm{H}}B^{\mathrm{T}}BF \circ \mathcal{T} + \mathcal{T} \circ F^{\mathrm{H}}F \circ \mathcal{T} \\ &= \mathcal{T} \circ F^{\mathrm{H}}(bI_L)F \circ \mathcal{T} + \mathcal{T} \circ I_L \circ \mathcal{T} \\ &= \mathcal{T} \circ bI_L \circ \mathcal{T} + I_M = (b+1)\,I_M. \end{aligned} \tag{17}$$

By substituting (17) into (16), $X^{(i+1)}$ is computed by

$$\begin{aligned} X^{(i+1)} = &\left(S^{\mathrm{H}}S + \frac{b+1}{\gamma}I_M\right)^{-1} \\ &\cdot \left(S^{\mathrm{H}}Y + \frac{1}{\gamma}\Big(\big(Z_1^{(i)\mathrm{T}} - D_1^{(i)\mathrm{T}}\big)B + Z_2^{(i)\mathrm{T}} - D_2^{(i)\mathrm{T}}\Big)F^{\mathrm{H}}\right). \end{aligned} \tag{18}$$

On the second line in (22), since the computation of $g(Z)$ is divided into $\nu\|Z_1\|_1^{G_2}$ and $\|Z_2\|_{1,\boldsymbol{\kappa}}^{G_3}$, $Z^{(i+1)}$ is computed by

$$\begin{cases} Z_1^{(i+1)} = \mathrm{prox}_{\gamma\nu\|\cdot\|_1^{G_2}}\big(BFX^{(i+1)\mathrm{T}} + D_1^{(i)}\big) \\ Z_2^{(i+1)} = \mathrm{prox}_{\gamma\|\cdot\|_{1,\boldsymbol{\kappa}}^{G_3}}\big(FX^{(i+1)\mathrm{T}} + D_2^{(i)}\big) \end{cases} \tag{19}$$

with the use of the proximity operators of the group ℓ_1-norms in (23). On the third line in (22), $D^{(i+1)}$ is computed by

$$\begin{cases} D_1^{(i+1)} = D_1^{(i)} + BFX^{(i+1)\mathrm{T}} - Z_1^{(i+1)} \\ D_2^{(i+1)} = D_2^{(i)} + FX^{(i+1)\mathrm{T}} - Z_2^{(i+1)} \end{cases} \tag{20}$$

and the solution of the problem in (15) is obtained by repeating (18)–(20) until a convergence condition is satisfied.

4 Numerical Experiments

To show the effectiveness of the proposed nonlinear beamforming, we conducted simulations based on the real reflection intensity, observed by the PAWR at Osaka University, in Fig. 2. At the range $r = 7.5\,[\mathrm{km}]$, we picked out 55 data between $\theta_{\min} = -15°\,[\mathrm{deg}]$ and $\theta_{\max} = 30°\,[\mathrm{deg}]$. The true reflection intensity $\boldsymbol{p}$ was created by the cubic spline interpolation of these 55 samples followed by adding Gaussian random numbers. We set $\lambda = 0.0318\,[\mathrm{m}]$, $d = 0.0165\,[\mathrm{m}]$, and $T_{\mathrm{PRT}} = 0.0004\,[\mathrm{s}]$. Random signals $\widetilde{\boldsymbol{x}}_m$ were generated in the frequency domain so that $E[|u_{m,l}|^2]$ would follow a Gaussian distribution wrapped into $[-\frac{1}{2T_{\mathrm{PRT}}}, \frac{1}{2T_{\mathrm{PRT}}}]$, on the basis of [10]. The mean Doppler frequency was generated from a uniform distribution $\mathcal{U}(-\frac{1}{2T_{\mathrm{PRT}}}, \frac{1}{2T_{\mathrm{PRT}}})$ for each elevation angle, and the Doppler frequency spectrum width was simply fixed to $\sigma = 125.7\,[\mathrm{Hz}]$. The standard division of $\boldsymbol{v}_l$ was set to $\sigma_v = \sqrt{5}$. For[1] $N = 128$ and $M = 110, 160$, we compared the proposed method with LS in (4),[2] FR in (5), MMSE in (8), and our previous method (Nonlinear I) in (12), in cases of $L = 20$. Note that CP in (6) is not compared since $\widehat{R}_y^{-1}$ cannot be computed. The parameters in (12) were set to $\nu_1 = 0.0025\frac{N\sqrt{qL}}{M}$ and $\nu_2 = 0.25\frac{N}{M\sqrt{b}}$. The group sizes of $\|\cdot\|_1^{G_1}$ and $\|\cdot\|_1^{G_2}$ were set to $q = 5$ for $M = 110$, $q = 8$ for $M = 160$, and $b = 3$. On the proposed method (Nonlinear II), the threshold was set to $\tau = 5$, and the parameters in (14) were set to $\nu = 0.25\frac{N}{M\sqrt{b}}$, $\kappa_{m,1} = 0.05\frac{N}{M\sqrt{\mathrm{card}(\boldsymbol{v}_m)}}$, and $\kappa_{m,2} = 12.5\frac{N}{M\sqrt{\mathrm{card}(\boldsymbol{v}_m^{\mathrm{C}})}}$, where card is the cardinal number.

Table 1 shows the average, for each situation, of the normalized errors $100\,\|\widehat{X} - X\|_{\mathrm{F}}/\|X\|_{\mathrm{F}}\,[\%]$ in 10 trials. From Table 1, we can see that the proposed method achieved the highest accuracy for both cases of $M = 110$ and $M = 160$. Figure 3(a) depicts the true power spectral density $E[|u_{m,l}|^2]$ in case of $M = 110$. Figures 3(b), 3(c), 3(d), 3(e), and 3(f) depict the estimated ones $|\widehat{u}_{m,l}|^2$ by LS, FR, MMSE, Nonlinear I, and Nonlinear II, respectively. From Figure 3, LS and FR failed in estimation particularly from 23° [deg] to 27° [deg] because the power spectral density should be 0 in this interval. MMSE reconstructed only a rough shape of the power spectral density and could not capture its fine shape. Nonlinear I greatly improved the estimation accuracy compared with the linear methods, but the support of the reconstructed power spectral density is slightly broad. The proposed method, Nonlinear II, reconstructed the power spectral density including its fine shape even from a few samples.

[1] When $M = 110$, the number of the sub-intervals, where signals exist, is $K = 93 < N$. On the other hand, when $M = 160$, the number of the sub-intervals is $K = 137 > N$, and hence it is very difficult to estimate X.

[2] To avoid the numerical instability in the computation of $S^{\dagger}$, we truncated the singular values of S that are smaller than 0.005.

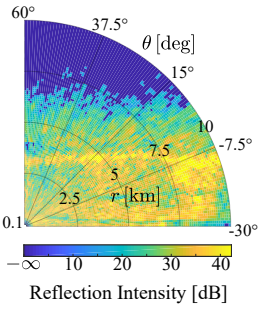

Figure 2: PAWR data.

Table 1: Mean of the normalized errors of each method in 10 trials.

Method	$\Delta\theta = \frac{45°}{110}$ $K = 93$ $L = 20$	$\Delta\theta = \frac{45°}{160}$ $K = 137$ $L = 20$
LS	76.96	83.28
FR	105.0	142.1
MMSE	72.73	118.1
Nonlinear I	22.23	49.54
Nonlinear II	**10.21**	**45.64**

5 Conclusion

In this paper, we have proposed a novel nonlinear beamforming method for a PAWR. The proposed method is an improved version of our previous nonlinear beamforming method, which utilizes group sparsity of the backscattered signals from distribute targets. Based on a rough estimation of the support of each power spectral density, we modified the previous convex cost function so that the power spectral densities of the optimal solution would have only one peak. Numerical experiments showed that the proposed method reconstructs the power spectral densities with higher accuracy compared to the linear and the previous nonlinear methods.

Appendix Alternating Direction Method of Multipliers

The alternating direction method of multipliers (ADMM) [8] solves the following convex optimization problem:

$$\underset{\boldsymbol{x}\in\mathcal{X},\,\boldsymbol{z}\in\mathcal{Z}}{\text{minimize}}\ f(\boldsymbol{x}) + g(\boldsymbol{z}) \qquad \text{subject to } \boldsymbol{z} = \mathcal{L}(\boldsymbol{x}), \tag{21}$$

where $\mathcal{X}$ and $\mathcal{Z}$ are finite-dimensional Hilbert spaces with the standard inner products, $\mathcal{L} : \mathcal{X} \to \mathcal{Z}$ is a linear mapping, and functions $f : \mathcal{X} \to \mathbb{R} \cup \{\infty\}$ and $g : \mathcal{Z} \to \mathbb{R} \cup \{\infty\}$ are proper, lower semicontinuous, and convex.[3] ADMM iteratively computes, from any initial value $(\boldsymbol{z}^{(0)}, \boldsymbol{d}^{(0)}) \in \mathcal{Z} \times \mathcal{Z}$,

$$\begin{cases} \boldsymbol{x}^{(i+1)} = \underset{\boldsymbol{x}\in\mathcal{X}}{\mathrm{argmin}}\ f(\boldsymbol{x}) + \dfrac{1}{2\gamma}\|\boldsymbol{z}^{(i)} - \mathcal{L}(\boldsymbol{x}) - \boldsymbol{d}^{(i)}\|_{\mathcal{Z}}^2 \\ \boldsymbol{z}^{(i+1)} = \mathrm{prox}_{\gamma g}(\mathcal{L}(\boldsymbol{x}^{(i+1)}) + \boldsymbol{d}^{(i)}) \\ \boldsymbol{d}^{(i+1)} = \boldsymbol{d}^{(i)} + \mathcal{L}(\boldsymbol{x}^{(i+1)}) - \boldsymbol{z}^{(i+1)} \end{cases} \tag{22}$$

for $i \geq 0$, and then $(\boldsymbol{x}^{(i)})_{i=1}^{\infty}$ converges to the optimal solution of the problem in (21), where $\gamma > 0$, $\|\cdot\|_{\mathcal{Z}}$ denotes the Euclidean norm introduced by the standard inner product in $\mathcal{Z}$, and $\mathrm{prox}_{\gamma g} : \mathcal{Z} \to \mathcal{Z}$ is the *proximity operator* defined by

$$\mathrm{prox}_{\gamma g}(\boldsymbol{y}) := \underset{\boldsymbol{z}\in\mathcal{Z}}{\mathrm{argmin}}\ g(\boldsymbol{z}) + \frac{1}{2\gamma}\|\boldsymbol{z} - \boldsymbol{y}\|_{\mathcal{Z}}^2.$$

If g is a group ℓ_1-norm with non-overlapping groups, from $g(\boldsymbol{z}) + \frac{1}{2\gamma}\|\boldsymbol{z} - \boldsymbol{y}\|_{\mathcal{Z}}^2 = \sum_{i=1}^{n_G}(\|\boldsymbol{z}_{\mathcal{G}_i}\|_2 + \frac{1}{2\gamma}\|\boldsymbol{z}_{\mathcal{G}_i} - \boldsymbol{y}_{\mathcal{G}_i}\|_2^2)$, the computation of $\mathrm{prox}_{\gamma g}$ is divided into those of $\mathrm{prox}_{\gamma\|\cdot\|_2}$. Therefore, $\mathrm{prox}_{\gamma\|\cdot\|_1^G}(\boldsymbol{y})$ can be computed for each group by

[3] A function $f : \mathcal{X} \to \mathbb{R} \cup \{\infty\}$ is called proper, lower semicontinuous, and convex if $\mathrm{dom}(f) := \{\boldsymbol{x} \in \mathcal{X} \mid f(\boldsymbol{x}) < \infty\} \neq \varnothing$, $\mathrm{lev}_{\leq\alpha}(f) := \{\boldsymbol{x} \in \mathcal{X} \mid f(\boldsymbol{x}) \leq \alpha\}$ is closed for all $\alpha \in \mathbb{R}$, and $f(\lambda\boldsymbol{x} + (1-\lambda)\boldsymbol{y}) \leq \lambda f(\boldsymbol{x}) + (1-\lambda)f(\boldsymbol{y})$ for all $\boldsymbol{x}, \boldsymbol{y} \in \mathcal{X}$ and all $\lambda \in (0, 1)$, respectively.

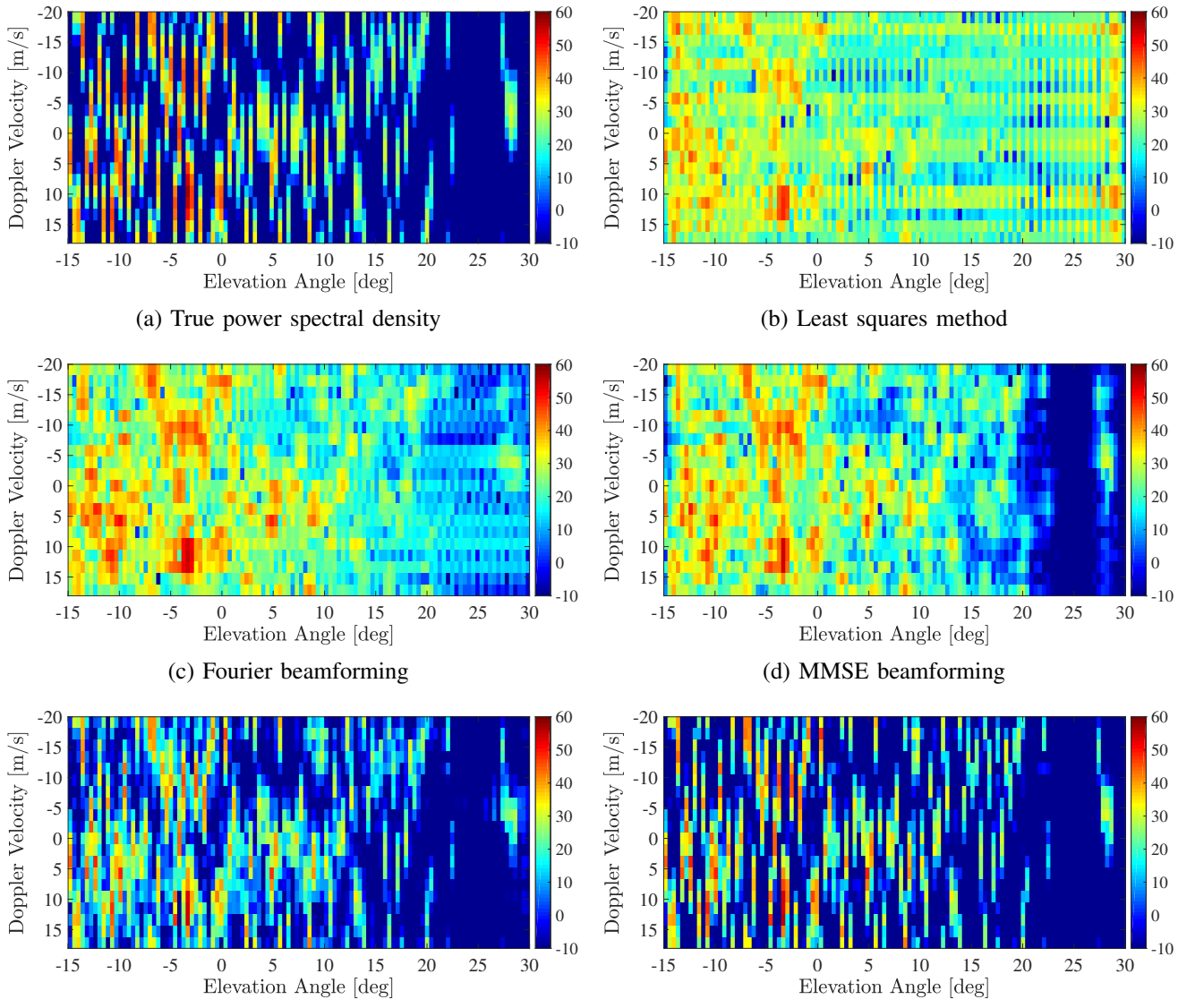

(a) True power spectral density

(b) Least squares method

(c) Fourier beamforming

(d) MMSE beamforming

(e) Nonlinear beamforming I

(f) Nonlinear beamforming II (proposed)

Figure 3: True power spectral density $E[|u_{m,l}|^2]$ [dB] and the estimated one $|\widehat{u}_{m,l}|^2$ by each method ($M = 110, L = 20$).

using the proximity operator of the ℓ_2-norm

$$\mathrm{prox}_{\gamma\|\cdot\|_2}(\boldsymbol{y}_{\mathcal{G}_i}) = \begin{cases} \dfrac{\|\boldsymbol{y}_{\mathcal{G}_i}\|_2 - \gamma}{\|\boldsymbol{y}_{\mathcal{G}_i}\|_2}\,\boldsymbol{y}_{\mathcal{G}_i} & \text{if } \|\boldsymbol{y}_{\mathcal{G}_i}\|_2 > \gamma, \\ \boldsymbol{0} & \text{if } \|\boldsymbol{y}_{\mathcal{G}_i}\|_2 \leq \gamma. \end{cases} \tag{23}$$

ACKNOWLEDGMENT

This work was supported in part by JSPS Grants-in-Aid for Research Activity Start-Up (Grant Number 17H07243).

REFERENCES

[1] B. Isom, R. Palmer, R. Kelley, J. Meier, D. Bodine, M. Yeary, B. L. Cheong, Y. Zhang, T. Y. Yu, and M. I. Biggerstaff, "The atmospheric imaging radar: Simultaneous volumetric observations using a phased array weather radar," *Journal of Atmospheric and Oceanic Technology*, vol. 30, no. 4, pp. 655–675, 2013.

[2] F. Mizutani, T. Ushio, E. Yoshikawa, S. Shimamura, H. Kikuchi, M. Wada, S. Satoh, and T. Iguchi, "Fast-scanning phased-array weather radar with angular imaging technique," *IEEE Transactions on Geoscience and Remote Sensing*, vol. 56, no. 5, pp. 2664–2673, 2018.

[3] E. Kudeki and F. Sürücü, "Radar interferometric imaging of field-aligned plasma irregularities in the equatorial electrojet," *Geophysical Research Letters*, vol. 18, no. 1, pp. 41–44, 1991.

[4] J. Capon, "High-resolution frequency-wavenumber spectrum analysis," *Proceedings of the IEEE*, vol. 57, no. 8, pp. 1408–1418, 1969.

[5] E. Yoshikawa, T. Ushio, Z. Kawasaki, S. Yoshida, T. Morimoto, F. Mizutani, and M. Wada, "MMSE beam forming on fast-scanning phased array weather radar," *IEEE Transactions on Geoscience and Remote Sensing*, vol. 51, no. 5, pp. 3077–3088, 2013.

[6] D. Kitahara, M. Nakahara, A. Hirabayashi, E. Yoshikawa, H. Kikuchi, and T. Ushio, "Nonlinear beamforming via convex optimization for phased array weather radar," in *Proc. APSIPA ASC 2018*, to appear.

[7] M. Wada, J. Horikomi, and F. Mizutani, "Development of solid-state weather radar," in *Proc. IEEE Radar Conference*, 2009, 4 pages.

[8] D. Gabay and B. Mercier, "A dual algorithm for the solution of nonlinear variational problems via finite elements approximations," *Computers & Mathematics with Applications*, vol. 2, no. 1, pp. 17–40, 1976.

[9] T. Y. Yu and M. B. Orescanin, "Beam multiplexing using the phased-array weather radar," *Journal of Atmospheric and Oceanic Technology*, vol. 24, no. 4, pp. 616–626, 2007.

[10] V. N. Bringi and V. Chandrasekar, *Polarimetric Doppler Weather Radar: Principles and Applications*. Cambridge University Press, 2001.

[11] S. Fukao and K. Hamazu, *Radar for Meteorological and Atmospheric Observations*. Springer Japan, 2014.